SANS characterization of particle dispersions in W-Ti and W-V alloys

A. Muñoz[a], M.A. Monge[a], B. Savoini[a], R. Pareja[a] and A. Radulescu[b]

[a]Departamento de Física. Universidad Carlos III de Madrid. 28911 Leganés, Spain

[b]Institut für Festköperforschung, Neutron Science JCNS, Outstation at FRM II, 85747 Garching, Germany

---

Abstract

SEM analyses of W-Ti and W-V alloys produced by a powder metallurgy route have revealed the presence of Ti or V pools with different sizes and shapes. The larger pools have sizes ranged between ~0.3 and several microns and are embedded between the matrix grains. The smaller Ti-rich (V-rich) particles, with sizes below ~0.3 μm, are spherical and they are dispersed inside the matrix grains. The characteristics of the second phase nanoparticles have been studied using the SANS technique. The scattering curves have been analyzed in terms of a polydisperse particle system following the Beaucage approach, and the maximum entropy method to obtain the particle size distributions. Beaucage analyses suggest the presence of two particle populations, characterized by radii of gyration from 50 to 80 Å (population I) and between 650 and 760 Å (population II). The volume distribution obtained by the maximum entropy approach reveals a prominent peak with particle diameter of 60 Å and ~70 Å for the W-Ti and W-V alloys, respectively. Secondary peaks in the size range 100 – 300 Å could be associated with the particle population with the larger radius of gyration.

Keywords: ODS alloys; refractory metals; SANS; HIP

* *Corresponding author:*angel.munoz@uc3m.es; tel. +34 916249413

1. Introduction

An important issue in the design of the future fusion reactor DEMO is the materials selection for a helium-cooled system of the first wall and blanket. W and its alloys are among the most promising structural and armor materials for building plasma facing components (PFCs) [1-6]. For accomplish their functions with reliance the properties of these materials such as the thermal conductivity, mechanical behavior at high temperature, recrystallization temperature, the ductile to brittle transition temperature (DBTT) and ductility have to be enhanced. Nevertheless, recent studies have demonstrated the difficulty of developing W alloys for PFCs [7]. Different strategies have been approached for achieving enhanced ductility in W alloys: solid solution alloying, grain refinement and nanostructuring as well as the use of W composites [8].

In the last years, W and several W-Ti and W-V alloys, with grain sizes of hundreds of nanometers and densification very close to 100%, have been produced by mechanical alloying and consolidation by hot isostatic pressing (HIP) [9-11]. In spite of the submicron grained microstructure, and a possible dispersion of second phase nanoparticles, these alloys do not exhibit a significant ductility enhancement. For instance, the W-4Ti alloy did not exhibit any sign of plastic flow up to 1273 K while unalloyed W processed following the same route did it at 673 K. For W-4V the DBTT is also very high, between 1073 and 1273 K [9, 12]. A relevant microstructural feature in the W-4Ti alloys that might give account for the mechanical behavior is the Ti segregation as large pools and dispersed particles with a wide range of sizes [13]. The same has been found for the W-V alloys despite the complete solid solution of V in W [11]. The aim of the present study has been to disclose the characteristics of the second phase nanoparticles dispersed in W-Ti and W-V alloys using the small angle neutron

scattering (SANS) technique. As this technique samples a macroscopic volume of material, it provides a more reliable and complete information about the size distribution of submicron-sized particles in a matrix than others as high-resolution transmission electron microscopy and atom probe tomography. In order to obtain reliable quantitative results the SANS data have been analyzed applying the Beaucage unified model [14,15] and the maximum entropy approach [16,17].

2 Experimental procedures

W-*x*wt%Ti and W-*x*wt%V alloys (*x*=2 and 4) were produced by a powder metallurgy route consisting in mechanical alloying of an elemental powder blend with the target composition and consolidation by HIP. The starting powders were: 99.9 % pure W, 99.9% pure Ti and 99.5 % pure V with particle sizes between 1 and 5 μm for W, <106 μm for Ti and <45 μm for V. The powder blends were mechanical alloyed for 20 h in a high-energy planetary mill. Then, the alloyed powder was canned and degassed, and consolidated for 2 h at 1575 K and 195 MPa. The details of the powder processing and consolidation have been reported elsewhere [11,13]. During the mechanical alloying X-ray diffraction measurements were performed on powder samples to monitor the alloying process. The oxygen content was also measured by IR absorption using a LECO ON836 analyzer. The density of the consolidated materials was determined with a He ultrapycnometer (Ultrapycnometer 1000). This device allows a very accurate volume measurement of the porous solids. This task is accomplished by employing Archimides' principle of fluid displacement and the Boyle law for an ideal gas. The morphology of the raw W,Ti and V powders was analyzed with a PHILIPS XL-30 scanning electron microscope. The microstructure of the alloys was studied using a high-resolution HITACHI S4800 J scanning electron microscope equipped with

an energy dispersive spectrometer (EDS). Fig. 1 shows the morphology of the starting elemental powders.

The SANS experiments were carried out in the KWS-2 spectrometer of the research reactor FRMII of the Jülich Centre for neutron Science (JCNS) at Garching (Germany) using a neutron wavelength of 7 Å. The samples had an area ~1.5×2.5 cm^2 and a thickness of ~2 mm. Data were acquired for sample-detector distance positions of 2, 8 and 20 m. These experimental conditions allowed cover the scattering vector range $0.002< Q <0.190$ $Å^{-1}$ corresponding to the angular range $0.068º< 2\theta <4.80º$ and scattering center sizes between ~30 and 3000 Å. The measured scattered intensity was corrected by subtracting the background counts and taking into account the detector efficiency. The resolution function of the instrument was also considered in the fitting procedure of the experimental data. The intensity was calibrated in absolute units using a Plexiglas sample as secondary reference standard to obtain the scattering cross section value $\Delta\Sigma/\Delta\Omega$ from the scattering centers embedded in the matrix.

3 Results and discussion

3.1 Sample characterization

Figs. 2 and 3 show the evolution of the X-ray diffraction patterns for W-4Ti and W-4V, respectively, during the fabrication process of the materials. After milling for 20 h, as well as in the consolidated materials, the diffraction peaks corresponding to α-Ti, (or V) observed in the starting blended powders were undetected and only those from bcc W were apparent. The same occurred for the W-2Ti and W-2V alloys.

The O contents in the alloys during the steps of the fabrication process, along with the densities, are presented in Table I. The O content in the W-V milled powders is

significantly higher than in the W-Ti ones, although it becomes similar after the consolidation process. This can be attributed to the higher O affinity of V. No evidence for oxides was detected in the X-ray diffraction patterns. The density measurements indicate that the consolidated alloys are virtually fully dense materials.

The microstructures of the W-2Ti and W-2V alloys are shown in Figs. 4 and 5, respectively. The matrix of the alloys exhibits a bimodal grain size distribution with modal values larger and smaller than 1 μm. A homogeneous distribution of irregular shaped pools of practically pure Ti or V appears in the consolidated alloys (dark areas in the images) as the EDS analyses reveals. The large pools, whose sizes ranged between ~0.3 and several microns, are found embedded between matrix grains. Besides, Ti-rich (V-rich) spherical particles with sizes smaller than ~0.3 μm are found dispersed inside the matrix grains as Figs. 4 and 5 reveal.

3.2 Small angle neutron scattering results

3.2.1 SANS data analyses

The experimental SANS data are usually plotted as the scattered intensity I versus the magnitude of the scattering vector Q. I is the differential cross-section per sample volume $d\Sigma/d\Omega$, and the scattering vector is $\boldsymbol{Q} = \boldsymbol{k'} - \boldsymbol{k}$, where $\boldsymbol{k'}$ and $\boldsymbol{k}$ are the wave-vectors of the scattered and incident neutrons, respectively. Q is related to the neutron wavelength λ and the scattering angle θ through the equation

$$Q = \frac{4\pi}{\lambda}\sin\theta \qquad (1)$$

where 2θ is the angle between $\boldsymbol{k'}$ and $\boldsymbol{k}$.

The I versus Q curve is usually adjusted according to a model-independent method. For low-Q scattering, the I versus Q curves follow the Guinier law (Guinier Regime)

$$I(Q) = Ge^{-\frac{Q^2 R_G^2}{3}} \tag{2}$$

where G is the scattering intensity at Q = 0 and R_G is the radius of gyration [18]. R_G provides a measure of the root mean square radius of the scattering centers dispersed in the matrix. For the high-Q scattering, the scattering curves can fulfill the Porod law (Porod Regime)

$$I(Q) = \frac{B}{Q^P} \tag{3}$$

The parameter B gives information about the number density, volume and scattering length density of scattering centers in the matrix [18]. The Porod exponent, P, provides information about the inner structure of the scattering centers such as the characteristics of their mass or surface organization. If $1< P <3$ the centers are mass fractal and their densities decrease as they grow; for $3< P <4$ the centers have a fractal surface, if $P > 4$ the centers exhibit a diffuse surface, and when P = 4 interface between the scattering center and the matrix would be a smooth surface [15, 19].

The Guinier and Porod local laws can be unified by the scattering Beaucage function for a single structural level [14]

$$I(Q) = G\exp\left(-\frac{Q^2 R_G^2}{3}\right) + \frac{B}{Q^P}\left[\mathrm{erf}\left(\frac{QR_G}{\sqrt{6}}\right)\right]^{3P} \tag{4}$$

This unified approach properly describes the small angle scattering from a polydisperse system over Q ranges of many orders of magnitude. G and B are Guinier and power-law pre-factors, respectively. P is the Porod exponent and erf() represents the error function

that provides a smooth transition between the Guinier (low Q scattering) and the Porod (high Q scattering) regimes, merging both regimes into a single function.

The present W-Ti and W-V alloys can be considered as dilute polydispersed systems. The matrix is the solvent and the solute phase is the Ti- or V-rich particles with sizes smaller than ~300 nm dispersed either inside the matrix grains or between the matrix grains. The high resolution SEM observations of these alloys point out that the size distribution of these particles does not correspond to a monomodal distribution. When several polydisperse levels are present and the particles scatter independently, the scattering curves can be approximated by the summation of independent Beaucage functions as given below [15]

$$I(Q) \cong \sum_{i=1}^{n} \left[G_i \exp\left(-\frac{Q_i^2 R_{G_i}^2}{3} \right) + \frac{B_i}{Q_i^P} \left[\operatorname{erf}\left(\frac{Q_i R_{G_i}}{\sqrt{6}} \right) \right]^{3P_i} \right] \tag{5}$$

where the i index refers to a particular region of the scattering curve, i.e. a single structural level for which the data fit a single exponential-power function, or unified scattering function.

A general determination of the size distribution of the scattering centers can be obtained resolving the following equation for the scattered intensity [20]

$$I(Q) = (\Delta\rho)^2 \int_0^\infty N(R) V^2(R) \left| F(Q,R) \right|^2 dR \tag{6}$$

where $\Delta\rho$ is the scattering contrast given by the difference between the neutron scattering length density for the scattering centers and the matrix, $N(R)$ the number density of centers with a radius between R and R+dR, and $V(R)$ and $F(Q, R)$ their volume and form factor. There are indirect transform methods for solving Eq. (6) and calculate the size distribution of the scattering centers if their shape is known to evaluate

$F(Q, R)$. These methods apply regularization techniques to get the smoothest possible solution, which require *a priori* assumptions about the solution [21].

Unlike the above methods, the maximum entropy approach can provide the most uniform size distribution histogram with the maximum configurational entropy being compatible with the scattering data [16, 17]. For obtaining the size distribution from the present SANS data, Eq. (6) has been solved with the IRENA 2.45 SAS package [22] using the maximum entropy algorithm developed in Ref. [17]. In the calculations the following scattering length densities for W, Ti and V were used: ρ_W=0.3072 ×10^{11} cm^{-2}, ρ_{Ti}=–0.19489 × 10^{11} cm^{-2} and ρ_V=–0.02619 × 10^{11} cm^{-2}.

3.2.2 Beaucage approach results

The experimental scattering data along with the fitted curves applying the Beaucage approach are represented in Fig. 6. The fitting of the curves were done using the software JCNS QtikWs [23]. In all cases, a polydisperse system and spherical scattering centers were assumed in reasonable agreement with the microstructure observed. For all the samples, the best fits were obtained by assuming two independent Beaucage functions represented by:

$$I(Q) = G_I \exp\left(-\frac{Q^2 R_{G_I}^2}{3}\right) + \frac{B_I}{Q^{P_I}}\left[\operatorname{erf}\left(\frac{QR_{G_I}}{\sqrt{6}}\right)\right]^{3P_I} + G_{II} \exp\left(-\frac{Q^2 R_{G_{II}}^2}{3}\right) + \frac{B_{II}}{Q^{P_{II}}}\left[\operatorname{erf}\left(\frac{QR_{G_{II}}}{\sqrt{6}}\right)\right]^{3P_{II}} \quad (7)$$

The fitting parameters are given in Table II. The respective background was subtracted in the fits. The results reveal two structural levels, or center populations, denoted as I and II. As it can be observed in Fig. 6, the first Beaucage function covers the range

$0.04<Q<0.19$ Å^{-1} (level I), whereas the second one covers the range $0.002<Q<0.04$ Å^{-1} (level II). This indicates a bi-modal distribution function for the scattering center sizes. Since the density measurements indicate that practically full densification was achieved in the alloys, scattering from small pores was considered negligible. So, the observed scattering characteristics are associated with the dispersion of the small Ti or V particles detected by SEM. The values of the radius of gyration, R_G, which are related to the typical size of the particles, range between 50 and 80 Å for the population I, and from 650 to 760 Å for population II. The particles exhibit a Porod exponent between 3.1 and 3.6 except for the populations of smaller size in the W-2Ti and W-4Ti alloys that have values of 2.36 and 2.05, respectively. This means that all the particles detected in the present SANS experiments have a surface fractal structure but in case of the W-Ti alloys those with the smaller radii of gyration, i.e. <55 Å appear to be mass fractal. A reasonable explanation for this divergent result cannot be given at present.

3.2.3. Particle size distribution results

The particle volume distributions as a function of the particle diameter are presented in Figs. 7 and 8. The distribution represented in these figures corresponds to the average values from ten solutions for Eq. (6) satisfying the criterion of maximum configurational entropy with a χ^2 value equal to the number of experimental data points. The error bars shown on each bin are the result of adding Gaussian noise to the measured intensities that is proportional to the experimental uncertainties. The four alloys exhibit very similar volume distribution functions characterized by a preponderant maximum, centered at ~60 Å for the W-Ti alloys or ~70 Å for the W-V alloys, and a sequence of three or four well defined secondary peaks in the diameter

range 100 – 300 Å. The possibility that these secondary peaks are artifacts of the maximum entropy approach can be rejected because the pattern resulted to be common for the four alloys. The corresponding positions of the peaks labeled as S_1, S_2 and S_3 coincide in W-2Ti and W-4Ti. In the W-V alloys the coincidences are less precise. The oscillations in the distributions in the range 300 – 2000 Å might be irrelevant because of the statistical uncertainties and error induced by approximating the scattering centers of this size range to spheres. The last can be responsible for the inconsistent fraction values of second phase obtained from the volume distributions for the W-V alloys. It is worth noting that the SEM analyses revealed the preferential presence of the smallest spherical particles in the inner of the matrix grains of the alloys while others laying at the grain boundaries and in the interstices between the W previous particles frequently exhibited a non-spherical shape.

Table III summarizes the results obtained from the volume distributions shown in Figs. 7 and 8. The correlation of the Beaucage approach results with the volume distribution of the dispersoids obtained by the maximum entropy method is not obvious. However, the R_G values of 50 – 80 Å, i.e. the root-mean-square (r.m.s) radii, for population I in the four alloys appear to be comparable with the cube-root-mean radii for the volume distribution that comprises up to particle diameters smaller than ~150 or 180 Å, i.e. up to the second definite valley in the distribution. The mean diameter values given in Table III are actually the ones that correspond with the mean volume for the volume distribution range considered, and therefore they are twice the cube-root-mean radii. In that case, the characteristics of population II could be associated with the wide tail of the volume distribution. The volume fraction of the second phase dispersed as nanoparticles in the matrix resulted to be two orders of magnitude smaller than the

nominal fraction in the alloy compositions. The remainder of the alloying element fraction is found as larger particles with sizes > 3000 Å and in solution in the W matrix.

4 Conclusions

The SANS measurements performed on samples of W-(2–4)Ti and W-(2–4)V alloys produced by powder metallurgy and HIP consolidation have confirmed the presence of a dispersion of particles in these materials with sizes smaller than ~200 nm. The analyses of the scattering curves in terms of a polydisperse particle system using the Beaucage approach suggest that this particle dispersion may consist of two structural levels, or particle populations, characterized by radii of gyration R_G of 50 to 80 Å (population I) and between 650 and 760 Å (population II). The analyses of the scattering data by the maximum entropy method yield volume distributions of the dispersoids characterized by an outstanding peak with modal particle diameters of 60 Å and ~70 Å for the W-Ti and W-V alloys, respectively. Besides, three secondary peaks are found defined in the size range 100 – 300 Å. The oscillations in the tail of the volume distributions may be an effect of the experimental errors and statistical uncertainties as well as by assuming a spherical shape for all the particles with sizes in that range.

The present results indicate that one has to be cautious if the Beaucage approach is applied to get information from polydisperse systems having maximums close to each other in the size distribution.

Acknowledgements

The SANS measurements were carried out at the neutron source Heinz Maier-Leibnitz (FRM II), Garching. The present work has been supported by the Ministerio de Economía y Competitividad of Spain (ENE2012-39787-C06-05) and by the Regional Government of Madrid through the programs S2013/MAE-2745 TECHNOFUSION(II)-CM and S2013/MIT-2862-MULTIMAT-CHALLENGE. The additional subvention from EURATOM/CIEMAT association through contract EFDA WP12-MAT-HHFM is also acknowledged. The authors thank the Microscopy Laboratory of CENIM-CSIC for the high resolution SEM measurements.

REFERENCES

[1] A. A. F. Tavassoli, J. Nucl. Mater. 302 (2002) 73–88.

[2] D. Maisonnier, D. Campbell, I. Cook, L. Di Pace, L. Giancarli, J. Hayward, A. Li Puma, M. Medrano, P. Norajitra, M. Roccella, P. Sardain, M.Q. Tran and D. Ward, Nucl. Fusion, 47 (2007) 1524-1532.

[3] J. Pamela, A. Bécoulet, D. Borba, J.-L. Boutard, L. Horton, D. Maisonnier, Fusion Eng. Des. 84 (2009) 194-204.

[4] V. Philipps, J. Nucl. Mater. 415 (2011) S2–S9.

[5] P. Norajitra, L.V. Boccaccini, E. Diegele, V. Filatov, A. Gervash, R. Giniyatulin, S. Gordeev, V. Heinzel, G. Janeschitz, J. Konys, W. Krauss, R. Kruessmann, S. Malang, I. Mazul, A. Moeslang, C. Petersen, G. Reimann, M. Rieth, G. Rizzi, M.

Rumyantsev, R. Ruprecht, V. Slobodtchouk, J. Nucl. Mater. 329–333 (2004) 1594–1598.

[6] P. Norajitra, S.I. Abdel-Khalik, L. M. Giancarli, T. Ihli, G. Janeschitz, S. Malang, I.V. Mazul and P.Sardain, Fusion Eng. Des. 83 (2008) 893-902.

[7] M. Rieth, S.L. Dudarev, et al., J. Nucl. Mater. 442 (2013) S173-S180.

[8] S. Wurster, N. Baluc, et al., J. Nucl. Mater. 442 (2013) S-181-S189.

[9] M.V. Aguirre, A. Martín, J.Y. Pastor, J. Llorca, M.A. Monge and R. Pareja, Metall. Mater. Trans. 40A (2009), 2283–2290.

[10] M.V. Aguirre, A. Martín, J.Y. Pastor, J. LLorca, M.A. Monge, R. Pareja, J. Nucl. Mater. 404 (2010) 203–209.

[11] A. Muñoz, M.A. Monge, B. Savoini, M.E. Rabanal, G. Garces, R. Pareja, J. Nucl. Mater. 417 (2011) 508 – 511.

[12]T. Palacios, J.Y. Pastor, M.V. Aguirre, A. Martin, M.A. Monge, A. Muñoz and R. Pareja, J. Nucl. Mater. 442 (2013 S277-S281.

[13] A. Muñoz, B. Savoini, E. Tejado, M.A. Monge, J.Y. Pastor, R. Pareja, J. Nucl. Mater. 455 (2014) 306–310.

[14] G. Beaucage, J. Appl. Cryst. 28 (1995) 717 – 728.

[15] G. Beaucage, J. Appl. Cryst. 29 (1996) 134 – 146.

[16] J. A. Potton, G. J. Daniell, B. D. Rainford, J. Appl. Cryst. 21 (1988) 891 – 897.

[17] P. R. Jemian, J.R. Weertman, G. G. Long and R. D. Spal, Acta Metall. Mater. 39 (1991) 24777–2487.

[18] G. Beaucage, H. K. Kammler, S. E. Pratsinis, J. Appl. Cryst. 37 (2004) 523 – 535.

[19] M.V. Avdeev, T.V. Tropin, V.L. Aksenov, L. Rosta, V.M. Garasmus, N.N. Rozhkova, Carbon 44 (2006) 954-961.

[20] O. Glatter, O. Kratky, Small angle X_Ray Scattering, London, Academic Press (1982).

[21] D. I. Svergun, J. Appl. Cryst. 25 (1992) 495 – 503.

[22] J. Ilavsky and P.R. Jemian, J. Appl. Cryst. 42 (2009) 347-353.

[23] V. Pipich, QtiKWS (2012), http://www.qtikws.de

TABLES

Table I. Oxygen contents in the W-Ti and W-V alloys. The theoretical density values ρ_{th} are calculated applying the mixing rule.

	Oxygen content (wt %)			**Density (g/cm^3)**		
	Blended	**Milling**	**HIP**	ρ_{th}	ρ_{exp}	**Densification**
W-2Ti	0.0814	0.123	0.208	18.069	18.116 ±0.003	100.2 %
W-4Ti	0.0858	0.103	0.267	17.069	17.160±0.003	100.5 %
W-2V	0.105	0.440	0.271	18.456	18.184±0.003	98.5 %
W-4V	0.180	0.542	0.280	17.725	17.581±0.003	99.2 %

Table II. Characteristic parameters obtained from the fits of the scattering curves using two independent Beaucage functions.

Population	Fitting parameters	W-2Ti	W-4Ti	W-2V	W-4V
I	R_g (Å)	53	51	54	80
	P	2.36	2.05	3.48	3.14
	G (cm^{-1})	0.7980	1.2729	0.7978	1.6985
	B (cm^{P-1})	68.824×10^{-6}	273.93×10^{-6}	2.714×10^{-6}	5.280×10^{-6}
II	R_g (Å)	703	757	653	675
	P	3.29	3.52	3.64	3.44
	G (cm^{-1})	4610	17610	4804	1902
	B (cm^{P-1})	5.407×10^{-6}	4.386×10^{-6}	1.479×10^{-6}	1.804×10^{-6}

Table III. Modal and mean diameters of second phase particles, and their volume fraction determined from the volume distribution obtained by the maximum of entropy method. (*) Mean value for the diameters that comprise the modal peak, and (**) mean value for the diameters that comprise up to the second valley in the distribution.

	W-2Ti	W-4Ti	W-2V	W-4V
Modal diameter (Å)	59	60	71	66
Mean* diameter (Å)	62	62	74	70
Mean** diameter (Å)	83	81	95	80
Volume (%)	0.19±0.02	0.45±0.05	0.50±0.05	0.24±0.04

FIGURE CAPTIONS

Figure 1. SEM images of the starting elemental powders.

Figure 2. X-ray diffraction patterns of W-4Ti blended powder, milled powder and consolidated sample. Inset: Enlargement of the diffraction pattern.

Figure 3. X-ray diffraction patterns of W-4V blended powder, milled powder and consolidated sample. Inset: Enlargement of the diffraction pattern.

Figure 4. HR-SEM image of W-2Ti showing spherical Ti-rich particles inside the matrix grains.

Figure 5. SEM image of W-2V showing V particles embedded between matrix grains.

Figure 6. Experimental SANS curves for the (a) W-Ti and (b) W-V alloys. The curves show the fit of the data points to two Beaucage functions.

Figure 7. Volume distribution of the second phase particles obtained by the maximum entropy approach for the W-2Ti and W-4Ti alloys with the corresponding normalized residuals for the fits.

Figure 8. Particle volume distribution obtained by the maximum entropy approach for the W-2V and W-4V alloys with the corresponding normalized residuals for the fits.

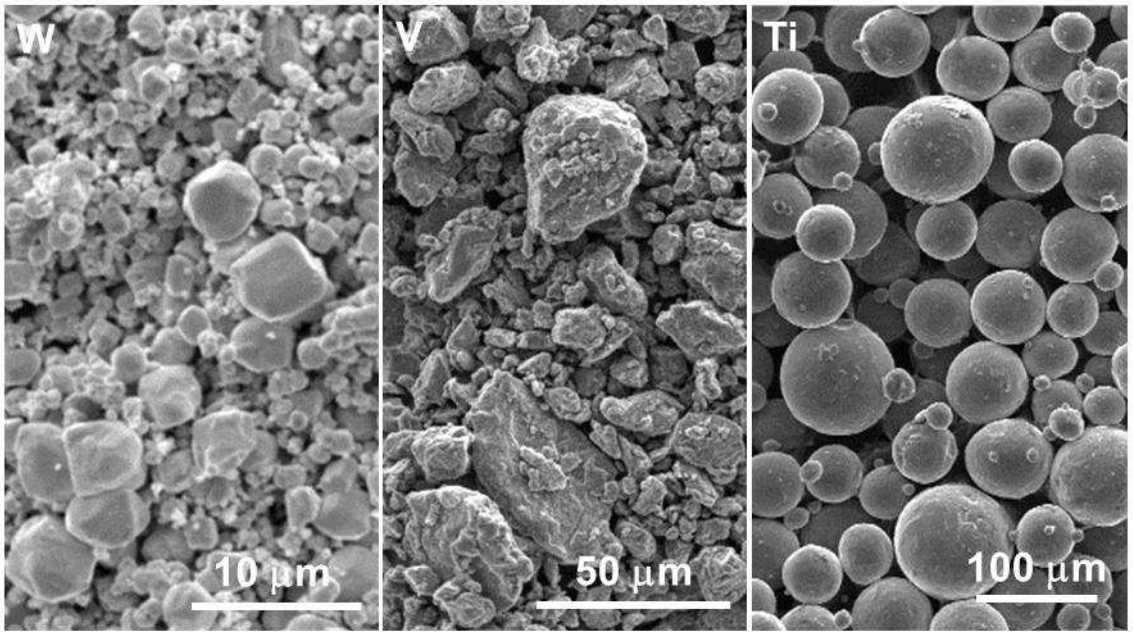

Figure 1

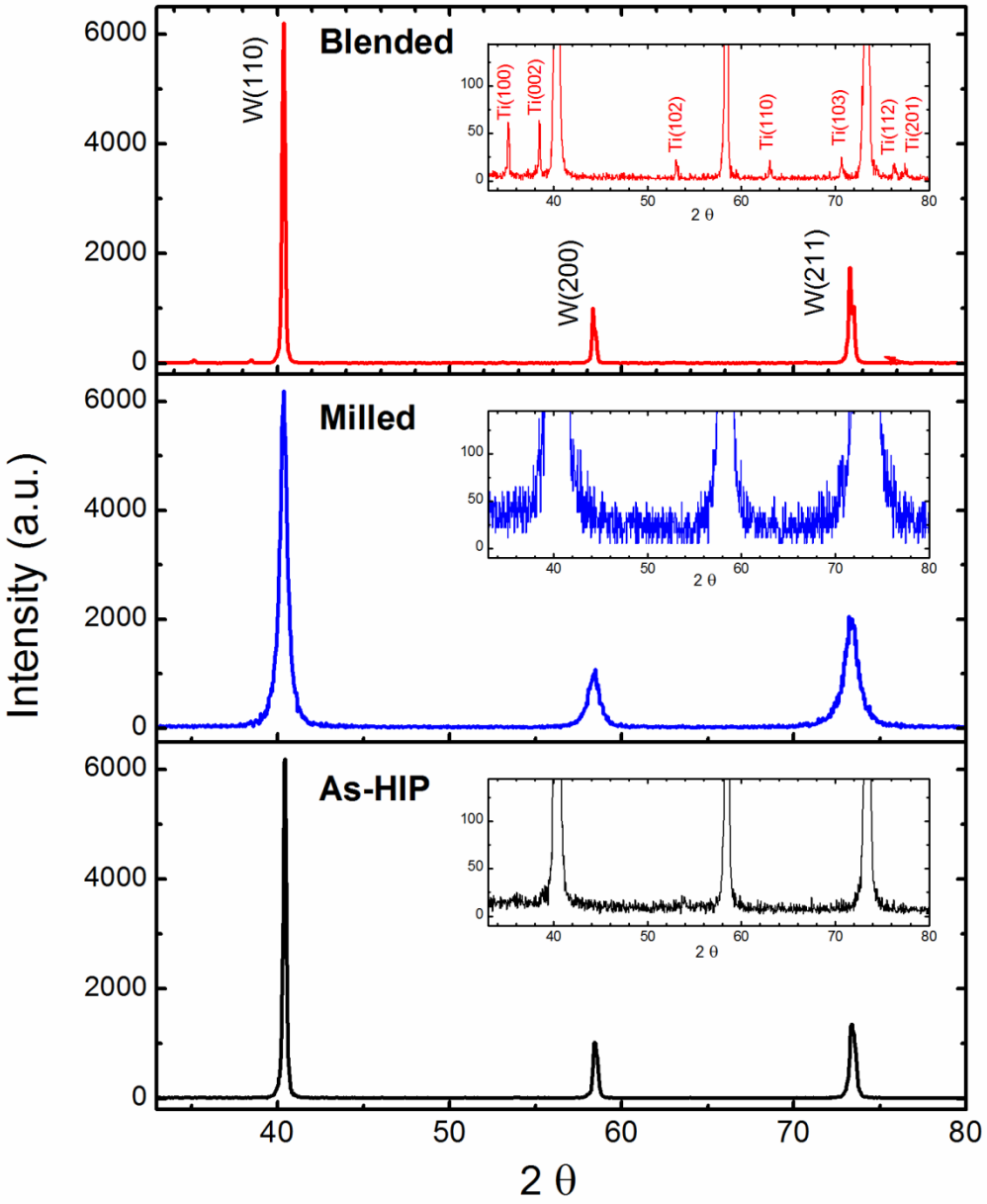
Blended
Milled
As-HIP
W(110)
W(200)
W(211)
Ti(100)
Ti(002)
Ti(102)
Ti(110)
Ti(103)
Ti(112)
Ti(201)
Intensity (a.u.)
2 θ

Figure 2

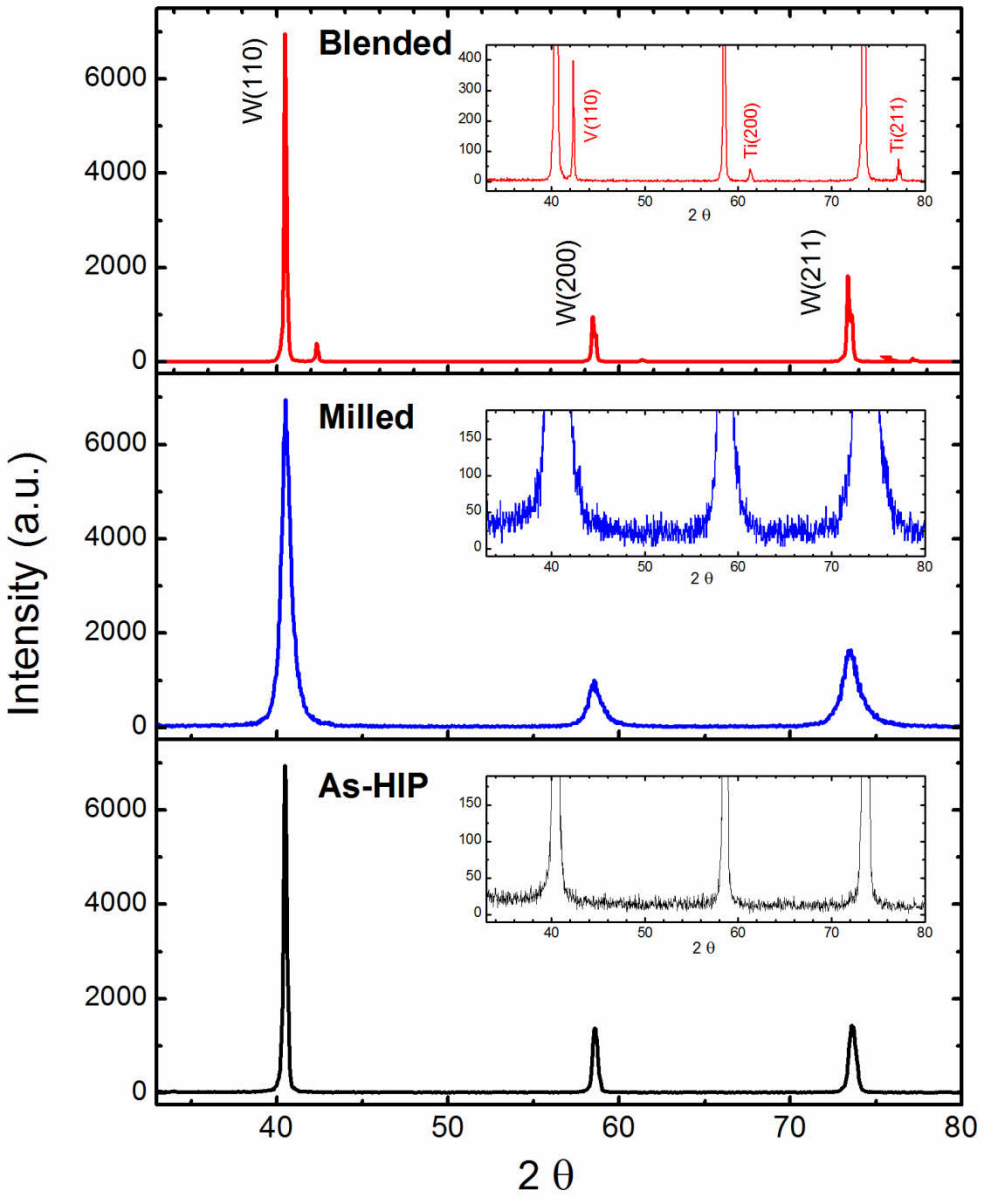
Blended
W(110)
W(200)
W(211)
V(110)
Ti(200)
Ti(211)
Milled
As-HIP
Intensity (a.u.)
2 θ

Figure 3

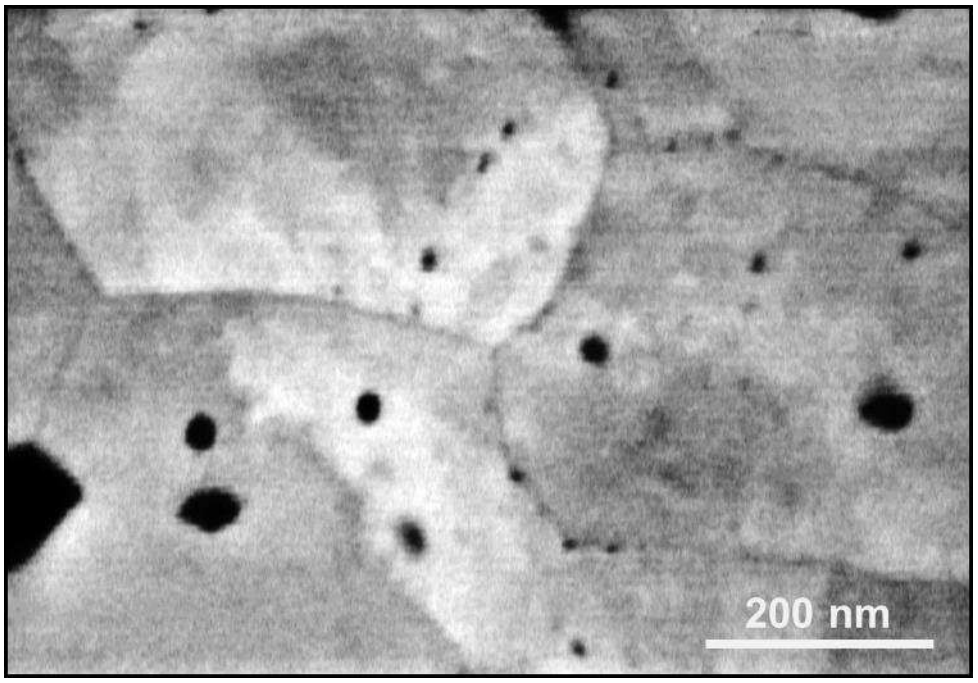

Figure 4

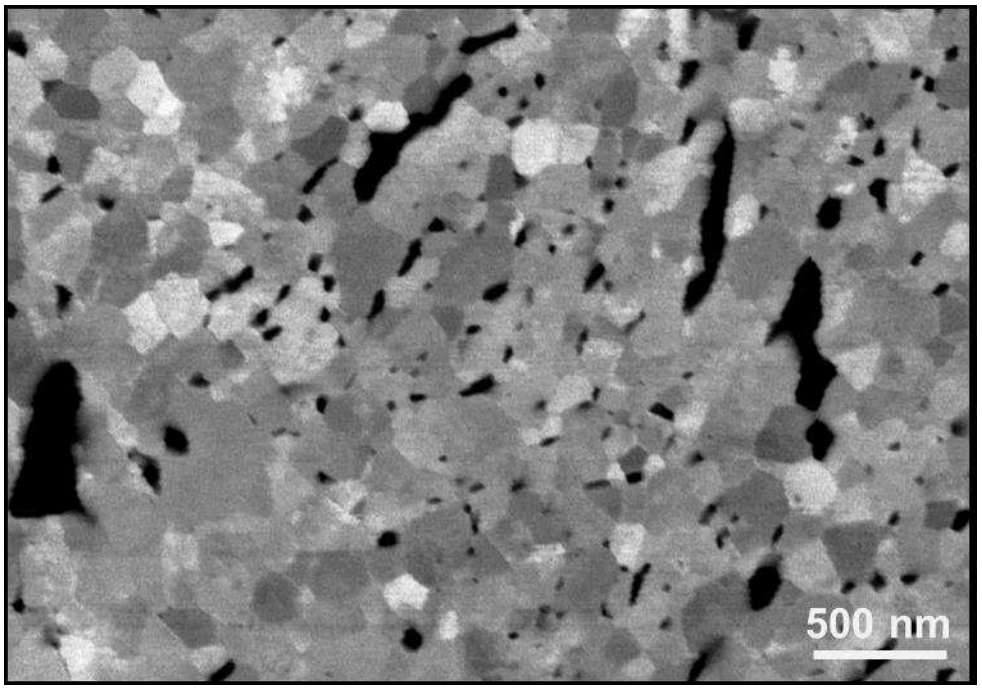

Figure 5

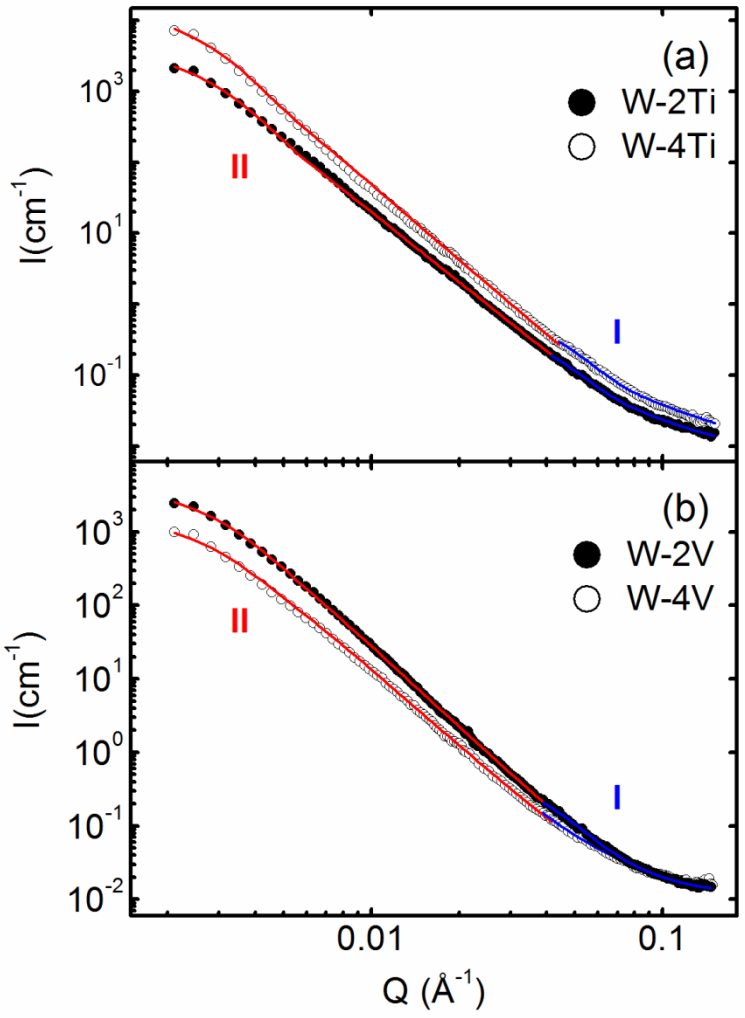
(a)
W-2Ti
W-4Ti
II
I
I(cm^{-1})
10^{3}
10^{1}
10^{-1}
(b)
W-2V
W-4V
II
I
I(cm^{-1})
10^{3}
10^{2}
10^{1}
10^{0}
10^{-1}
10^{-2}
0.01
0.1
Q (Å^{-1})

Figure 6

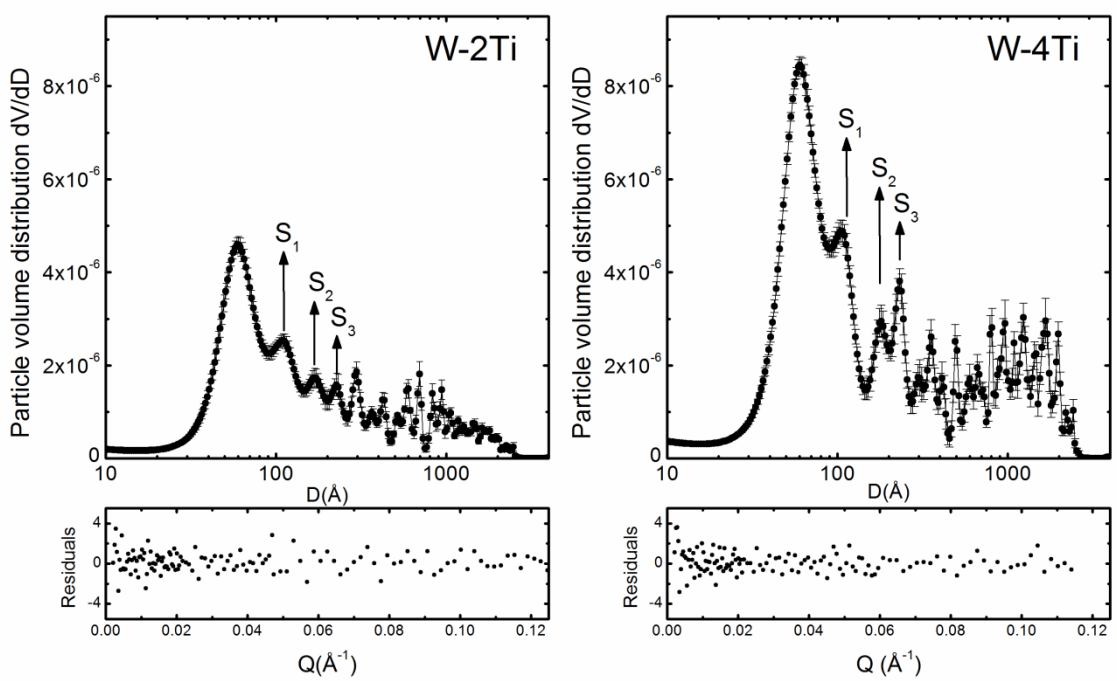

Figure 7

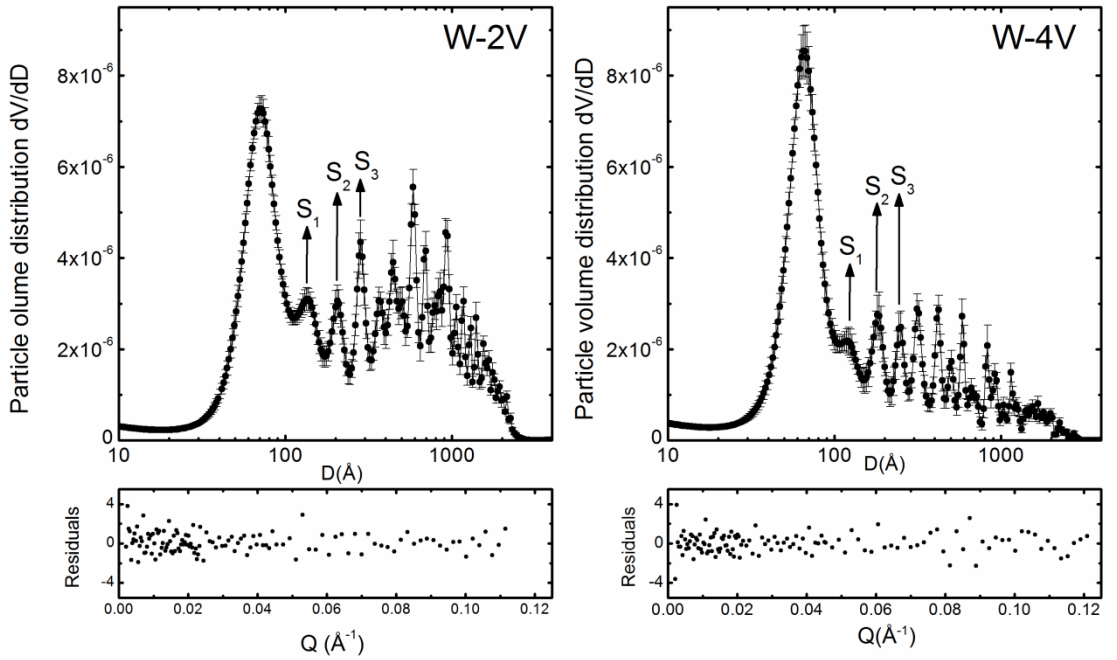

Figure 8